

Microkinetic Modeling of Ethane Hydrogenolysis on Metals

I. V. Kuz'min and A. V. Zeigarnik

Zelinskii Institute of Organic Chemistry, Russian Academy of Sciences, Moscow, 119991 Russia

Received November 13, 2003

Abstract—The microkinetic analysis of ethane hydrogenolysis in the framework of the Sinfelt–Taylor mechanism is carried out using UBI–QEP data on the energetics of elementary steps. On single-crystalline surfaces of Pd(111), Pt(111), and Ni(111), the reaction predominantly occurs via ethyl formation in which the C–C bond is cleaved. The surface concentration of ethylidyne is very low, and ethyl has the highest concentration among all hydrocarbon fragments. For the conditions studied in this work, the activity in ethane hydrogenolysis increases in the series Pd(111) < Pt(111) < Ni(111). According to the results of kinetic modeling, the reaction occurs via quasi-equilibrium steps of adsorption and dissociation of hydrogen and ethane and further, practically irreversible formation of methane.

INTRODUCTION

Ethane hydrogenolysis is one of the oldest model reactions of heterogeneous catalysis whose mechanism is still debatable. Many researchers agree that the reaction occurs via the Sinfelt–Taylor mechanism [1–15], which consists of the following steps: hydrogen chemisorption, ethane dehydrogenation on the catalyst surface with the formation of adsorbed C_2H_x species, the C–C bond cleavage in C_2H_x ($x = 5–0$) with the formation of CH_y species ($y = 3–0$), and CH_y hydrogenation with the formation of methane, which desorbs from the surface. At the same time, some authors assume that this mechanism is not applicable to all catalysts [16]. Those who accept the Sinfelt–Taylor mechanism believe that the rate is determined by C–C bond cleavage in the fragments formed via quasi-equilibrium steps.

The main Sinfelt's argument [1, 2] in favor of the proposed mechanism is based on experimental data that hydrocarbons are chemisorbed on the metal surface with the formation of gaseous hydrogen at lower temperatures than those necessary for hydrogenolysis. The results of H/D exchange under hydrogenolysis conditions may provide further evidence for the proposed mechanism since they suggest that the reactivity of C–H bonds is higher compared to that of C–C bonds although the energy of C–C bonds is ~ 10 kcal/mol lower. The reason for such a reactivity pattern is that the binding energies (chemisorption heats) of intermediates with the catalyst surface determine the activation energy estimates of the corresponding elementary steps together with the C–C and C–H bond strengths.

Analyzing the kinetics of ethane hydrogenolysis in the framework of the proposed model, Sinfelt presumed that the number of hydrogen atoms in C_2H_x frag-

ments where the C–C bond is cleaved differs for different catalysts [1–3]:

Metal	Co	Ni, Ru, Os, Ir	Rh, Pd, Pt
x	4	2	0

Sinfelt assumed the absence of competition between ethane and hydrogen for the active sites on the surface, and this assumption was criticized by Boudart [17].

In some papers another step of C–C bond cleavage assisted by surface hydrogen was considered [2, 18, 19]:



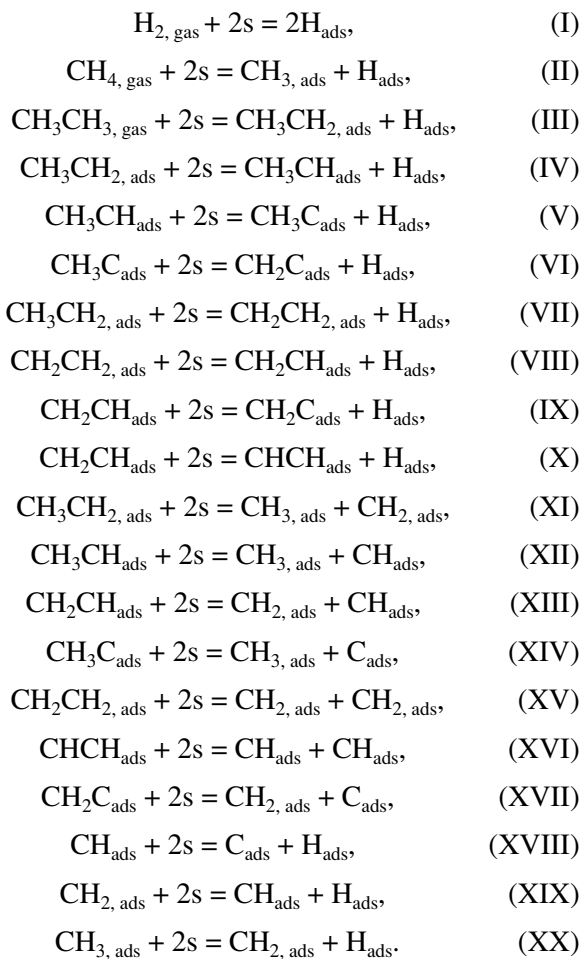
Arguments were also presented for considering the steps of hydrogen atom transfer from one carbon atom bound to the surface to another such atom in another surface species [20]. It is possible that steps of other types are also missing in the mechanisms that are proposed most frequently.

For the Sinfelt–Taylor mechanism, the key questions remain: In what surface compound is the C–C bond cleaved, what pathway contributes the most to the overall rate, and do the C–C bond cleavage steps determine the rate? It also remains unclear whether the most important routes depend on the nature of the catalyst surface.

Earlier, these issues were addressed by estimating the activation energies of C–C bond cleavage steps in possible intermediates [21, 22] by the unity bond index–quadratic exponential potential (UBI–QEP) method proposed by Shustorovich and Sellers [23–25]. However, these estimates did not provide clear answers to the above questions. There were only reasons to assume that the most probable species where the C–C bond is cleaved are ethyl, ethylidyne, adsorbed acetylene, CH_2CH_{ads} , CH_2C_{ads} , and CHC_{ads} . Moreover, the calculation procedure used in [21, 22] was rather com-

plex and provided qualitatively sound results, but they conflicted with other numeric values used in the UBI-QEP approach. Finally, the methods for calculating the binding energies of some key intermediates in ethane hydrogenolysis were improved in the recent work [26].

In this work, we took standard UBI-QEP numeric values of input parameters [26] and improved calculation techniques for the binding energies of some adsorbed species [26]. Then, we carried out kinetic modeling based on the Sinfelt-Taylor mechanism, using a computer program that we developed without the assumption of the quasi-equilibrium of steps. The mechanism presented below includes all possible C-C bond cleavage steps:



METHODS

Program for Kinetic Modeling

We developed a computer program for kinetic modeling for the Microsoft Windows platform with a convenient user interface. The program makes it possible to compose rate laws based on a set of elementary steps with activation energies and preexponential factors. Based on these data, the program generates a set of differential equations in a form that is compact and convenient for simulation. The main working part of the pro-

gram solves the system of stiff differential equations and consists of several modules:

(1) A subprogram for calculating the values of the rates using the vector of concentrations and the Jacobian matrix and other derivatives by real-time differentiation of the set of equations.

(2) The main module that implements several methods for solving the set of stiff differential equations, including the Rosenbrock method with various sets of parameters [27–29], the method of semi-implicit extrapolation [30], various modifications of the Gear method (BDF) [31, 32], and Adams–Moulton formulas (AMF) [33]. In addition to these methods, we implemented and improved the CVODE program package [34]. The code of functions was rewritten and optimized.

(3) The subprogram for estimating the sensitivity coefficients for kinetic equations with respect to various parameters.

(4) The external shell for estimating the ranges of computation (time and number of iterations), checking the fulfillment of equilibrium and stationary regimes, showing results at a graphical display, and writing various files (binary, text, MS Excel spreadsheets, etc.).

The choice of the above methods for kinetic modeling is explained by the stiffness of the set of differential equations that describe the evolution of the kinetic system over time. The stiffness is typical for many kinetic problems in heterogeneous catalysis and appears when dependent variables change depending on two or more independent variables with substantially different coefficients.

In this work all simulations were carried out using the Rosenbrock method and 80-digit registers of a coprocessor.

Microkinetic Modeling

To model kinetics, we entered the reaction mechanism, the activation energies of elementary steps calculated by the UBI-QEP method (see below), and the values of the preexponential factors. The latter were obtained assuming that they are independent of the catalyst. We took the values of preexponential factors from the published models [4, 5]. They were assumed to be equal to $1.0 \times 10^{13} \text{ s}^{-1}$ for the surface reactions and desorption; a value of $1.0 \times 10^6 \text{ kPa}^{-1} \text{ s}^{-1}$ was taken for hydrogen adsorption; and a value of $1.0 \times 10^4 \text{ kPa}^{-1} \text{ s}^{-1}$ was taken for ethane and methane adsorption. The partial pressures of gases (methane, ethane, and hydrogen) were considered constant for each simulation experiment. The pressures of hydrogen and ethane were varied from 0.1 to 1 atm and from 0.01 to 0.1 atm, respectively. The pressure of methane was taken equal to zero. The temperature range was 478–673 K.

Simulations were carried out for the plug-flow reactor working in the regime of low conversions up to the steady state. The absolute admissible error in calculat-

ing the concentrations was 1×10^{-50} , and the relative admissible error was 1×10^{-6} . According to simulations, the steady-state values of the rates were achieved for approximately 1 h. The initial integration step was chosen to be 10^{-20} s. The scale of time was set by the values of the preexponential factors. As a result, the surface coverages with various species, the rates of each reactant formation, and the rates of each step were recorded. The accuracy of simulations was checked using the balance of free surface and the balance of the rates of elementary steps in the steady state.

Activation Energy Calculations by the UBI-QEP Method

To calculate the activation energies of elementary steps on the surfaces of Ni(111), Pd(111), and Pt(111), we used the UBI-QEP method in the zero-coverage limit [23–26]. The input data were the binding energies of atomic adsorbates on these metals obtained in experiments or reliable calculations. When calculating the activation energies, the binding energies of adsorbates are calculated first, which in turn are calculated from the values of two-center metal–element bonds Q_0 . The latter are constants and can be taken from [26].

To calculate the binding energies of H and C (Q_H and Q_C) on the above surface, we used the following formula:

$$Q_A = Q_0(2 - 1/n), \quad n = 3, \quad A = H, C. \quad (1)$$

The values of ethane binding energies were taken from [22], and the corresponding values for methane were taken 1.5 kcal/mol lower than for ethane.

In the case of strong binding of adsorbate X ($X = \text{CH}_3\text{CH}, \text{CH}_3\text{C}, \text{CH}_2, \text{CH}$) with the surface via atom A (in our case $A = C$), the following equation is used:

$$Q_X = Q_A^2 / (Q_A + D_{AB}), \quad (2)$$

where D_{AB} is the sum of bond energies between an atom that binds X to the surface and the rest of a molecule. For CH_3CH , CH_3C , CH_2 , and CH , D_{AB} is 173, 114 (the average between the limiting values in two partitioning schemes [35]), 183 and 81 kcal/mol, respectively; $Q_A = Q_C$. In the case of medium-strength binding, we used the formula

$$Q_X = 0.5 \left(\frac{Q_{0A}^2}{Q_{0A}/n + D_{AB}} + \frac{Q_A^2}{Q_A + D_{AB}} \right), \quad (3)$$

where $X = \text{CH}_3\text{CH}_2$, CH_3 and $D_{AB} = 283$ and 293 kcal/mol, respectively; n corresponds to the position of an adsorbate; in our case $n = 1$. The binding of H_2 is calculated according to the formula

$$Q_{A_2} = \frac{9Q_{0A}^2}{6Q_{0A} + 16D_{A_2}}, \quad A = H, \quad (4)$$

where D_{H_2} is the H–H bond energy (104 kcal/mol). The binding energies of symmetric molecules XX (where $X = \text{CH}$ and CH_2) were calculated according to the formulas proposed in [26]:

$$Q_{XX} = \frac{9Q_X^2}{6Q_X + 16D}, \quad (5)$$

where $Q_X = Q_{\text{CH}}$ and Q_{CH_2} , and D is the sum of bond energies in the gaseous acetylene (392 kcal/mol) and ethylene (538 kcal/mol), respectively. The binding energies of CH_2C and CHC where one of the carbon atoms has no bonds with a hydrogen atom were calculated using the standard formula:

$$Q_X = \frac{ab(a+b) + D_{AB}(a-b)^2}{ab + D_{AB}(a+b)}. \quad (6)$$

In Eq. (6), D_{AB} is the C–C bond energy ($D_{\text{CH}_2\text{C}} = 155$ kcal/mol and $D_{\text{CHC}} = 161$ kcal/mol). The values of a and b for the first and second contact atoms were found as follows. For the contact carbon atom without hydrogen substituents, this is simply the value of Q_{0C} (that is, $b = Q_{0C}$). For the contact carbon atom with m hydrogen substituents, their effect is taken into account according to the formula [26]

$$a, b = Q_{0C} \left(1 - \left(\frac{mQ_{0H}}{mQ_{0C} + Q_{0H}} \right)^2 \right). \quad (7)$$

For the CH_2CH species, the binding energy is calculated using formula (6), the value of a is calculated using formula (7) where $m = 2$ and b is calculated using formula (7) where $m = 1$. The C–C bond energy is 157 kcal/mol. In all calculations we assumed that C_2 species (except for ethylidyne, ethylidene, and ethyl) are bound via two contact atoms to the surface.

All steps in the Sinfelt–Taylor mechanism are of the form $\text{AB}_{\text{ads}} = \text{A}_{\text{ads}} + \text{B}_{\text{ads}}$. The activation energies of such steps are calculated using the formula

$$E = 0.5[\Delta H + Q_A Q_B / (Q_A + Q_B)], \quad (8)$$

where ΔH is the enthalpy of the reaction on the metal surface calculated from the thermodynamic cycle desorption–gas-phase reaction–adsorption:

$$\Delta H = Q_{AB} + D - Q_A - Q_B. \quad (9)$$

In Eq. (9), D is enthalpy of the analogous gas-phase reaction estimated from the bond energies:

$$D = D_{AB} - D_A - D_B. \quad (10)$$

The activation energy of the reverse reaction is calculated from the conditions

$$E_{\text{reverse}} = E_{\text{forward}} - \Delta H. \quad (11)$$

Table 1. Binding energies of adsorbates (kcal/mol) in ethane hydrogenolysis

Species	Metal		
	Ni(111)	Pd(111)	Pt(111)
H _{ads}	63.0	62.0	61.0
C _{ads}	171.0	160.0	150.0
CH ₃ CH ₃ , ads	7.7	7.7	7.6
CH ₃ CH ₂ , ads	48.8	43.5	38.9
CH ₃ CH _{ads}	85.0	76.9	69.7
CH ₃ C _{ads}	102.6	93.4	85.2
CH ₂ CH ₂ , ads	14.7	12.7	11.0
CH ₂ CH _{ads}	43.3	37.9	33.3
CH ₂ C _{ads}	47.1	41.6	36.9
CHCH _{ads}	20.6	18.0	15.7
CHC _{ads}	46.6	41.3	36.6
CH ₄ , ads	6.2	6.2	6.1
CH ₃ , ads	47.6	42.4	37.9
CH ₂ , ads	82.6	74.6	67.6
CH _{ads}	116.0	106.2	97.4
H ₂ , ads	6.8	6.6	6.4

If the activation energy appears to be negative, we introduce the thermodynamic correction: this activation energy is set equal to zero and the activation energy of the reverse reaction is chosen so that Eq. (11) is fulfilled.

RESULTS AND DISCUSSION

The results of calculations by the UBI–QEP method are shown in Tables 1 and 2.

Surface Coverages

To calculate the surface coverages, we chose the constant values of the partial pressures of hydrogen (20.26 kPa) and ethane (3.04 kPa) at 478 K. These conditions are typical of ethane hydrogenolysis on all three surfaces under study. Simulations were carried out until reaching a steady state. The simulated values of surface coverages by hydrogen and hydrocarbon species (in

fractions of unity) for these conditions are presented in Table 3.

As can be seen from Table 3, the main portion of the surface is covered by hydrogen, and this fact agrees with data presented in [36, 37]. Of all the hydrocarbon fragments, ethyl dominates on any of the three surfaces. Therefore, in contrast to common assumptions, the surface coverages are not proportional to the binding strengths of the corresponding species. Thus, ethyl is more abundant than ethylidyne on the surface, although ethylidyne species are bound more strongly than ethyl. The authors of [36, 37] draw another picture: ethylidyne and di- σ -bonded ethylene dominate, whereas the surface concentration of ethyl species was reported to be insignificant. The authors of [36, 37] concluded that ethylidyne is the most abundant and ethyl is the most reactive on the Pt(111) surface. That is, according to their data, the most reactive species does not necessarily have the highest concentration. In our simulations, the surface concentration of CH₂CH₂ is rather high, but it is several orders of magnitude lower than the concentration of ethyl. One of the hypothetical precursors of C–C bond cleavage, ethylidyne has a rather low concentration on palladium, whereas it is comparable with the concentration of CH₂CH₂ on nickel.

The results of calculations allowed us to calculate the reaction orders in ethane and hydrogen and the apparent activation energy of the overall reaction under the following conditions: $P_{H_2} = 0.1\text{--}1$ atm, $P_{C_2H_6} = 0.01\text{--}0.1$ atm, and $T = 478\text{--}560$ K. These data are summarized in Table 4. This table also presents reference data for comparison. Simulations showed that the apparent reaction order in ethane on all metals under consideration is equal to unity, and the order in hydrogen is close to -2 . These orders can be explained as follows.

The authors of [37] showed that, in the framework of the considered scheme, a decrease in the order of hydrogen compared to -2 is due to the lateral interactions between strongly adsorbed hydrocarbon fragments and atomic hydrogen. These lateral interactions can be described by the coadsorption model [24] of the UBI–QEP method that predicts a decrease in the binding energies of a species and the corresponding changes in the activation energies of reactions in which they participate according to Eq. (8). Since we used the zero-coverage limit values of the binding and activation energies, lateral interactions were neglected. The reaction order corresponds to the condition of equilibrium between adsorbed C₂H_x species and ethane. Thus, without taking into account changes in the activation energies, we obtained reaction orders that qualitatively agree with published data, and better agreement with the experiment is seemingly indistinguishable in the framework of such a model.

The apparent activation energies agree well with published data for Pd. For Ni, the agreement is acceptable assuming all the uncertainties of the calculation

scheme. In the case of Pt, there is much discrepancy in the published data. Some of the experimental values agree well with the results of our simulations.

Rates of Steps and Reaction Routes

To calculate the rate of each step, we took the following conditions: hydrogen partial pressure, 20.26 kPa; ethane partial pressure, 3.04 kPa; 478 K. Simulations were carried out until reaching the steady state. The results are presented in Table 5.

It can be seen from Table 5 that the reaction largely occurs via a single route with the C–C bond cleavage in ethyl (steps (I)–(III), (XI), (X)), and all other routes can be neglected. Indeed, under steady-state conditions the rates of the elementary steps meet the following condition: $r_I = r_{III} = r_{XI} = -r_{XX} = r_{II}/2$. It is easy to check that this condition is fulfilled with the following relative errors: 0.1% for Ni, 0.8% for Pt, and 0.2% for Pd. Thus, according to our simulations, the ethyl species is both the most reactive of all C_2 species and the most abundant one. If we take any of the rates of a step from the above route, we can estimate the relative activity of metals under steady-state conditions: Ni \gg Pt $>$ Pd. This activity series coincides with that reported for metals supported on SiO_2 [1], as well as with both experimental [38] and theoretical [21, 22, 38] data for single-crystalline surfaces. For platinum we carried out five additional simulation experiments where we varied the ratio of the partial pressures of hydrogen and ethane (10/1, 1/1, 1/10, 1/1000). The partial pressures were varied in the range 60–60000 Pa. In all cases, the route with C–C bond cleavage in ethyl contributed most greatly to the overall reaction rate.

We simulated the forward and reverse rates of the elementary steps in the route with C–C bond cleavage in ethyl (Table 6). These data allow us to judge the applicability of the rate-limiting step approximation. This approximation assumes that steps other than rate-limiting are quasi-equilibrium, in which case the concentrations of intermediate species can be expressed in terms of the partial pressures of methane, ethane, and hydrogen and the equilibrium constants. Data presented in Table 6 show that, for all single-crystalline surfaces under consideration, steps (I) and (III) are indeed quasi-equilibrated (the forward and reverse rates are equal to each other). Step (II) is not quasi-equilibrated since our model assumes that the partial pressure of methane is equal to zero (the model of low conversion). According to simulations, steps (XI) and (XX) are not equilibrium steps. Therefore, the approximation of the rate-limiting step is not applicable to ethane hydrogenolysis modeling. At the same time, several researchers used an approximation supported by the results of this work according to which the steps of C_2H_x formation are quasi-equilibrated, whereas the formation of methane from C_2H_x is practically irreversible [1, 3, 39–41]. For all surfaces under consideration, the first practically irreversible step is C–C bond cleavage.

Table 2. Activation energies of steps in the forward and reverse directions and the enthalpies of reactions (kcal/mol) in ethane hydrogenolysis

Step	Metal					
	Ni(111)		Pd(111)		Pt(111)	
	forward reaction	reverse reaction	forward reaction	reverse reaction	forward reaction	reverse reaction
(I)	1.3	23.3	2.2	22.2	3.0	21.0
(II)	13.9	19.5	16.0	15.4	20.2	25.1
(III)	10.7	24.5	12.9	20.4	14.7	25.1
(IV)	23.5	12.7	24.5	9.8	25.4	7.1
(V)	24.2	14.8	24.4	12.9	24.5	11.1
(VI)	23.7	3.2	21.4	3.5	19.2	3.8
(VII)	10.5	1.4	8.7	1.9	7.1	2.2
(VIII)	25.5	0.1	29.8	0.0	33.7	0.0
(IX)	16.6	10.4	16.1	8.8	15.7	7.3
(X)	2.1	13.4	0.4	13.5	0.0	14.4
(XI)	24.4	5.8	26.8	0.3	33.4	0.0
(XII)	23.6	10.2	25.3	5.1	26.8	0.5
(XIII)	24.9	23.3	29.0	14.9	32.6	7.3
(XIV)	2.1	35.1	3.8	29.8	5.3	25.0
(XV)	31.4	9.9	36.4	0.9	47.9	0.0
(XVI)	38.3	19.7	44.3	8.8	50.9	0.0
(XVII)	7.1	48.6	11.4	39.5	15.4	31.1
(XVIII)	4.5	41.5	5.0	39.7	5.4	38.0
(XIX)	23.2	17.6	23.8	15.4	24.3	13.2
(XX)	23.9	11.9	24.8	9.0	25.7	6.3

Table 3. Surface coverages by various species and the fraction of the free surface (in the fractions of unity) under steady-state conditions at $P_{H_2} = 20.26$ kPa, $P_{C_2H_6} = 3.04$ kPa, and $T = 478$ K

Species	Metal		
	Pt(111)	Pd(111)	Ni(111)
H_{ads}	0.94884551	0.98153421	0.99347747
CH_3, ads	$4.2188784 \times 10^{-13}$	$1.2089241 \times 10^{-17}$	$1.3074811 \times 10^{-13}$
CH_3CH_2, ads	4.7702802×10^{-7}	2.8370506×10^{-9}	2.6555401×10^{-7}
CH_3CH_{ads}	$5.6487083 \times 10^{-18}$	$1.8729972 \times 10^{-19}$	$1.3115863 \times 10^{-16}$
CH_3C_{ads}	$5.2003268 \times 10^{-27}$	$5.9568382 \times 10^{-29}$	$1.0214901 \times 10^{-26}$
CH_2C_{ads}	$1.3517551 \times 10^{-36}$	1.386658×10^{-40}	$1.8292768 \times 10^{-40}$
CH_2CH_2, ads	$7.5634697 \times 10^{-12}$	$7.6663605 \times 10^{-16}$	$7.8536929 \times 10^{-16}$
CH_2CH_{ads}	$8.1453703 \times 10^{-30}$	$6.3126299 \times 10^{-33}$	8.189924×10^{-32}
$CHCH_{ads}$	8.61923×10^{-26}	$2.1411447 \times 10^{-30}$	$5.1466585 \times 10^{-31}$
CH_2, ads	$5.3662291 \times 10^{-22}$	$7.1639017 \times 10^{-21}$	$2.1903837 \times 10^{-17}$
CH_{ads}	$2.2707482 \times 10^{-27}$	$1.2216444 \times 10^{-28}$	$2.9891388 \times 10^{-25}$
C_{ads}	$3.4721665 \times 10^{-15}$	$3.1202162 \times 10^{-17}$	$6.2065576 \times 10^{-15}$
Free surface	0.051154014	0.018465789	0.0065222683
Maximal unbalance	9.9×10^{-9}	6.73×10^{-9}	3.07×10^{-9}

Table 4. The apparent reaction orders in ethylene and hydrogen and the apparent activation energy of ethane hydrogenolysis in various systems (comparison of experimental and simulated data)

System	T, K	P_{H_2}, atm	$P_{C_2H_6}, atm$	n_{H_2}	$n_{C_2H_6}$	$E_a, kcal/mol$	Reference
Ni/SiO ₂	450–492	0.2	0.03	−2.4	1	40.6	[1, 2]
Ni(111)	520–600	0.13	0.0013	–	–	46.1	[38]
Ni(111)	478–650	0.1–1	0.01–0.1	−1.9	1	52.4	This work
Pd/SiO ₂	616–650	0.2	0.03	−2.5	0.9	58	[1, 2]
Pd/SiO ₂	478	0.20	0.01–0.10	−2.6	1	56.7	[5]
Pd(111)	478–650	0.1–1	0.01–0.1	−1.8	1	55.5	This work
Pt/SiO ₂	344–385	0.2	0.03	−2.5	0.9	54	[1, 2]
Pt(111)	550–640	0.13	0.0013			36.6	[38]
	570–625	0.13	0.0013			43.5	[38]
	473–623	0.13	0.013	−0.55	1.2	34	[45]
Pt/SiO ₂	478	0.20	0.01–0.10	−2.5	1	55.3	[5]
Pt(111)	478–650	0.1–1	0.01–0.1	−2	1	59	This work

Table 5. The rates of elementary steps under steady-state conditions at $P_{H_2} = 20.26$ kPa, $P_{C_2H_6} = 3.04$ kPa, and $T = 478$ K

Step	Rate, s^{-1}		
	Pt(111)	Pd(111)	Ni(111)
(I)	6.67×10^{-12}	5.40×10^{-12}	7.88×10^{-10}
(II)	-1.34×10^{-11}	-1.08×10^{-11}	-1.58×10^{-9}
(III)	6.70×10^{-12}	5.40×10^{-12}	7.88×10^{-10}
(IV)	5.96×10^{-19}	5.45×10^{-21}	1.37×10^{-18}
(V)	5.13×10^{-19}	3.72×10^{-21}	4.65×10^{-19}
(VI)	-8.24×10^{-27}	-8.08×10^{-31}	-8.65×10^{-31}
(VII)	-1.08×10^{-17}	-1.06×10^{-22}	-3.88×10^{-20}
(VIII)	8.24×10^{-27}	8.08×10^{-31}	5.56×10^{-31}
(IX)	8.24×10^{-27}	8.08×10^{-31}	8.64×10^{-31}
(X)	3.52×10^{-33}	-2.01×10^{-37}	3.79×10^{-37}
(XI)	6.68×10^{-12}	5.40×10^{-12}	7.88×10^{-10}
(XII)	8.24×10^{-20}	1.73×10^{-21}	9.04×10^{-19}
(XIII)	2.65×10^{-34}	1.18×10^{-36}	1.44×10^{-34}
(XIV)	5.13×10^{-19}	3.72×10^{-21}	4.64×10^{-19}
(XV)	2.49×10^{-23}	5.95×10^{-23}	1.47×10^{-21}
(XVI)	1.20×10^{-38}	4.06×10^{-41}	6.74×10^{-40}
(XVII)	3.22×10^{-33}	2.90×10^{-36}	4.42×10^{-35}
(XVIII)	6.27×10^{-20}	1.94×10^{-21}	1.11×10^{-18}
(XIX)	-1.98×10^{-20}	2.21×10^{-22}	2.03×10^{-19}
(XX)	-6.68×10^{-12}	-5.40×10^{-12}	-7.88×10^{-10}

CONCLUSION

Based on the microkinetic analysis of the Sinfelt–Taylor mechanism of ethane hydrogenolysis using data obtained by the UBI–QEP method, we draw the following conclusions:

On the single-crystalline surfaces of Pd(111), Pt(111), and Ni(111) at 478 K and partial pressures of hydrogen and ethane equal to 20.26 and 3.04 kPa, respectively, the reaction of ethane hydrogenolysis mostly occurs via the formation of surface ethyl where a C–C bond is cleaved. All other routes can be neglected in the steady state. This conclusion agrees with data reported in [37] where Monte Carlo modeling using parameters calculated by the DFT method suggested that the main reaction route on Pt includes C–C bond cleavage in ethyl and that the surface is mostly covered by hydrogen. However, in our case the concentration of ethylidyne on the surface is very low, which is in contrast to the result reported in [37] where ethylidyne was reported to have the highest surface concentration of all hydrocarbon fragments. It was assumed in [42] that the C–C bond cleavage in the surface ethyl is assisted by surface hydrogen: $C_2H_5,_{ads} + H,_{ads} \rightarrow 2CH_3,_{ads}$. We assume that this step has a low probability because the transition state of this elementary step is too complex and has a strained geometry.

Based on the analysis carried out in this paper, we can rank the relative activities of the surfaces Pd(111), Pt(111), and Ni(111) as was done in [43] using analogous methods for the water-gas shift reaction. Under the conditions considered in this paper, the activity toward ethane hydrogenolysis increases in the series Pd(111) < Pt(111) < Ni(111), and this activity series agrees with our data and data from other researchers [21, 22, 38, 44].

Table 6. The rates of elementary steps (in reciprocal seconds) in the forward and reverse directions under steady-state conditions at $P_{H_2} = 20.26$ kPa, $P_{C_2H_6} = 3.04$ kPa, and $T = 478$ K

Step	Metal					
	Ni(111)		Pd(111)		Pt(111)	
	forward reaction	reverse reaction	forward reaction	reverse reaction	forward reaction	reverse reaction
(I) $H_2,_{gas} + 2s = 2H,_{ads}$	219.3050	219.3050	681.5336	681.5336	2252.856458	2252.856458
(II) $CH_4,_{gas} + 2s = CH_3,_{ads} + H,_{ads}$	0	1.576771×10^{-10}	0	1.079168×10^{-11}	0	1.336982×10^{-11}
(III) $CH_3CH_3,_{gas} + 2s = CH_3CH_2,_{ads} + H,_{ads}$	1.657287×10^{-5}	1.657208×10^{-5}	1.310534×10^{-5}	1.310533×10^{-5}	1.511725×10^{-5}	1.511724×10^{-5}
(XI) $CH_3CH_2,_{ads} + 2s = CH_3,_{ads} + CH_2,_{ads}$	7.883855×10^{-10}	6.383653×10^{-20}	5.395839×10^{-12}	6.315127×10^{-25}	6.684912×10^{-12}	2.263947×10^{-21}
(XX) $CH_3,_{ads} + 2s = CH_2,_{ads} + H,_{ads}$	6.571009×10^{-16}	7.88386×10^{-10}	1.888141×10^{-19}	5.395839×10^{-12}	1.960454×10^{-14}	6.704517×10^{-12}

The reaction occurs through the quasi-equilibrium steps of ethane and hydrogen adsorption and further irreversible conversion of intermediate species into methane.

REFERENCES

1. Sinfelt, J.H., *Adv. Catal.*, 1973, vol. 23, p. 91.
2. Sinfelt, J.H., *Catal. Rev.*, 1970, vol. 3, p. 175.
3. Sinfelt, J.H., *J. Catal.*, 1972, vol. 27, p. 468.
4. Goddard, S.A., Amiridis, M.D., Rekoske, J.E., Cardona-Martinez, N., and Dumesic, J.A., *J. Catal.*, 1989, vol. 117, p. 155.
5. Dumesic, J.A., Rudd, D.F., Aparicio, L.M., Rekoske, J.E., and Treviño, A.A., *The Microkinetics of Heterogeneous Catalysis*, Washington, DC: Am. Chem. Soc., 1993.
6. Bond, G.C., Hooper, A.D., Slaa, J.C., and Taylor, A.O., *J. Catal.*, 1996, vol. 163, p. 319.
7. Guczi, L., Gudkov, B.S., and Tetenyi, P., *J. Catal.*, 1972, vol. 24, p. 187.
8. Tanaka, K., Miyazaki, T., and Aomura, K., *J. Catal.*, 1983, vol. 81, p. 328.
9. Smale, M.W. and King, T.S., *J. Catal.*, 1990, vol. 125, p. 335.
10. Gudkov, B.S., Guczi, L., and Tetenyi, P., *J. Catal.*, 1982, vol. 74, p. 207.
11. Engstrom, J.R., Goodman, D.W., and Weinberg, W.H., *J. Am. Chem. Soc.*, 1988, vol. 110, p. 8305.
12. Rodriguez, J.A. and Goodman, W.D., *J. Phys. Chem.*, 1990, vol. 94, p. 5342.
13. Martin, G.A., *J. Catal.*, 1979, vol. 60, p. 345.
14. Wang, P.-K., Slichter, C.P., and Sinfelt, J.H., *J. Phys. Chem.*, 1990, vol. 94, p. 1154.
15. Ko, E.I. and Garten, R.L., *J. Catal.*, 1981, vol. 68, p. 233.
16. Frennet, A., Degols, L., Lienard, G., and Grucq, A., *J. Catal.*, 1974, vol. 35, p. 18.
17. Boudart, M., *AIChE J.*, 1972, vol. 18, p. 465.
18. Mahaffy, P. and Hansen, R.S., *J. Chem. Phys.*, 1979, vol. 71, p. 1853.
19. Chen, B. and Goodwin, J.G., Jr., *J. Catal.*, 1995, vol. 154, p. 1.
20. Zeigarnik, A.V., Valdés-Pérez, R.E., and Egorova, N.I., *Surf. Sci.*, 2001, vol. 487, p. 146.
21. Zeigarnik, A.V. and Myatkova, O.N., *Kinet. Katal.*, 2001, vol. 42, no. 3, p. 464.
22. Zeigarnik, A.V., Valdés-Pérez, R.E., and Myatkova, O.N., *J. Phys. Chem. B.*, 2000, vol. 104, no. 45, p. 10578.
23. Shustorovich, E., *Adv. Catal.*, 1990, vol. 37, p. 101.
24. Shustorovich, E., *Surf. Sci. Rep.*, 1986, vol. 6, p. 1.
25. Shustorovich, E. and Sellers, H., *Surf. Sci. Rep.*, 1998, vol. 31, p. 1.
26. Shustorovich, E. and Zeigarnik, A.V., *Surf. Sci.*, 2003, vol. 527, nos. 1–3, p. 137.
27. Kaps, P. and Rentrop, P., *Numerische Math.*, 1979, vol. 33, p. 55.
28. Shampine, L.F., *ACM Trans. Math. Soft.*, 1979, vol. 8, p. 93.
29. Bieniasz, L.K., *J. Electroanal. Chem.*, 1999, vol. 469, p. 97.
30. Bader, G. and Deuflhard, P., *Numerische Math.*, 1983, vol. 41, p. 373.
31. Gear, C.W. *Numerical Initial Value Problems in Ordinary Differential Equations*, Englewood Cliffs: Prentice-Hall, 1971.
32. Gear, C.W. and Wells, R.R., *Multirate Linear Multistep Methods.*, 1984, vol. 24, p. 484.
33. Gupta, G.K. and Wallace, C.S., *Math. Comp.*, 1975, vol. 29, no. 130, p. 489.
34. Cohen, S.D. and Hindmarsh, A.C. *CVODE User Guide*, Lawrence Livermore National Laboratory Report UCRL-MA-118618, September 1994.
35. Shustorovich, E. and Bell, A.T., *Surf. Sci.*, 1988, vol. 205, p. 492.
36. Cortright, R.D., Watwe, R.M., and Dumesic, J.A., *J. Mol. Catal. A: Chem.*, 2000, vol. 163, p. 91.
37. Podkolzin, S.G., Alcalá, R., Pablo, J.J., and Dumesic, J.A., *J. Phys. Chem. B.*, 2002, vol. 106, p. 9604.
38. Rodriguez, J.A. and Goodman, D.W., *Surf. Sci. Rep.*, 1991, vol. 14, nos. 1–2, p. 1.
39. Sinfelt, J.H., Taylor, W.F., and Yates, D.J.C., *J. Phys. Chem.*, 1965, vol. 69, p. 95.
40. Cimino, A., Boudart, M., and Taylor, H.S., *J. Phys. Chem.*, 1954, vol. 58, p. 796.
41. Cortright, R.D., Watwe, R.M., Spiewak, B.E., and Dumesic, J.A., *Catal. Today.*, 1999, vol. 53, p. 395.
42. Larsson, R., *Catal. Lett.*, 1992, vol. 13, p. 71.
43. Zeigarnik, A.V., Callahan, C., Datta, R., Fishtick, I., and Shustorovich, E., *Kinet. Katal.*, in press.
44. Frese, K.W., Jr., *Surf. Sci.*, 1987, vol. 182, nos. 1–2, p. 85.
45. Zaera, F. and Somorjai, G.A., *J. Phys. Chem.*, 1985, vol. 89, p. 3211.